Compensation of spatial inhomogeneities in a cavity soliton laser using a spatial light modulator

Neal Radwell,[1] Patrick Rose,[2] Carsten Cleff,[2] Cornelia Denz,[2] and Thorsten Ackemann[1,*]

[1]*Department of Physics and SUPA, University of Strathclyde, John Anderson Building, 107 Rottenrow East, Glasgow, G4 0NG, UK*

[2]*Institut für Angewandte Physik and Center for Nonlinear Science (CeNoS), Westfälische Wilhelms-Universität Münster, Corrensstraße 2/4, 48149 Münster, Germany*

[*]*thorsten.ackemann@strath.ac.uk*

Abstract: Dissipative solitons are self-localized states which can exist anywhere in a system with translational symmetry, but in real systems this translational symmetry is usually broken due to parasitic inhomogeneities leading to spatial disorder, pinning the soliton positions. We discuss the effects of semiconductor growth induced spatial disorder on the operation of a cavity soliton laser based on a vertical-cavity surface-emitting laser (VCSEL). We show that a refractive index variation induced by an external, suitably spatially modulated laser beam can be used to counteract the inherent disorder. In particular, it is demonstrated experimentally that the threshold of one cavity soliton can be lowered without influencing other cavity solitons making two solitons simultaneously bistable which were not without control. This proof of principle paves the way to achieve full control of large numbers of cavity solitons at the same time.

OCIS codes: (190.6135) Spatial solitons; (190.1450) Bistability; (190.5970) Semiconductor nonlinear optics including MQW; (190.4420) Nonlinear optics, transverse effects in.

References and links

1. G. I. Stegeman and M. Segev, "Optical spatial solitons and their interactions: universality and diversity," Science **286**, 1518–1523 (1999).
2. M. Segev, "Solitons: a universal phenomenon of self-trapped wave packets," Opt. Photonics News **13**, 27 (2002). Introduction to special issue on *Solitons*.
3. S. Barland, J. R. Tredicce, M. Brambilla, L. A. Lugiato, S. Balle, M. Giudici, T. Maggipinto, L. Spinelli, G. Tissoni, T. Knödel, M. Miller, and R. Jäger, "Cavity solitons as pixels in semiconductors," Nature **419**, 699–702 (2002).
4. N. Akhmediev and A. Ankiewicz, eds., *Dissipative solitons*, vol. 661 of *Lecture Notes in Physics* (Springer, Berlin, 2005).
5. T. Ackemann, G.-L. Oppo, and W. J. Firth, "Fundamentals and applications of spatial dissipative solitons in photonic devices," Adv. Atom. Mol. Opt. Phys. **57**, 323–421 (2009).
6. F. Lederer, G. I. Stegeman, D. N. Christodoulides, G. Assanto, M. Segev, and Y. Silberberg, "Discrete solitons in optics," Phys. Rep. **463**, 1–126 (2008).
7. Y. Tanguy, T. Ackemann, and R. Jäger, "Characteristics of switching in a semiconductor based cavity-soliton laser," Opt. Express **15**, 16773–16780 (2007).
8. Y. Tanguy, T. Ackemann, W. J. Firth, and R. Jäger, "Realization of a semiconductor-based cavity soliton laser," Phys. Rev. Lett. **100**, 013907 (2008).
9. Y. Tanguy, N. Radwell, T. Ackemann, and R. Jäger, "Characteristics of cavity solitons and drifting excitations in broad-area vertical-cavity surface-emitting lasers with frequency-selective feedback," Phys. Rev. A **78**, 023810 (2008).

#129452 - $15.00 USD Received 4 Jun 2010; revised 11 Aug 2010; accepted 11 Aug 2010; published 19 Oct 2010

10. P. Genevet, S. Barland, M. Giudici, and J. R. Tredicce, "Cavity soliton laser based on mutually coupled semiconductor microresonators," Phys. Rev. Lett. **101**, 123905 (2008).
11. N. Radwell and T. Ackemann, "Characteristics of laser cavity solitons in a vertical-cavity surface-emitting laser with feedback from a volume Bragg grating," IEEE J. Quantum Electron. **45**, 1388–1395 (2009).
12. T. Elsass, K. Gauthron, G. Beaudoin, I. Sagnes, R. Kuszelewicz, and S. Barbay, "Fast manipulation of laser localized structures in a monolithic vertical cavity with saturable absorber," Appl. Phys. B **98**, 327–331 (2010).
13. N. N. Rosanov, "Switching waves, autosolitons, and parallel digital-analogous optical computing," Proc. SPIE **1840**, 130–143 (1991).
14. W. J. Firth and A. J. Scroggie, "Optical bullet holes: robust controllable localized states of a nonlinear cavity," Phys. Rev. Lett. **76**, 1623–1626 (1996).
15. B. Schäpers, T. Ackemann, and W. Lange, "Characteristics and possible applications of localized structures in an optical pattern–forming system," Proc. SPIE **4271**, 130–137 (2001).
16. C. Cleff, B. Gütlich, and C. Denz, "Gradient induced motion control of drifting solitary structures in a nonlinear optical single feedback experiment," Phys. Rev. Lett. **100**, 233902 (2008).
17. F. Pedaci, S. Barland, E. Caboche, P. Genevet, M. Giudici, J. R. Tredicce, T. Ackemann, A. J. Scroggie, W. J. Firth, G.-L. Oppo, G. Tissoni, and R. Jäger, "All-optical delay line using semiconductor cavity solitons," Appl. Phys. Lett. **92**, 011101 (2008).
18. S. Barbay, X. Hachair, T. Elsass, I. Sagnes, and R. Kuszelewicz, "Homoclinic snaking in a semiconductor-based optical system," Phys. Rev. Lett. **101**, 253902 (2008).
19. P. Genevet, B. Barland, M. Giudici, and J. R. Tredicce, "Stationary localized structures and pulsing structures in a cavity soliton laser," Phys. Rev. A **79**, 033819 (2009).
20. R. Kuszelewicz, I. Ganne, I. Sagnes, and G. Slekys, "Optical self-organization in bulk and multiquantum well gaalas microresonators," Phys. Rev. Lett. **84**, 6006–6009 (2000).
21. E. Caboche, F. Pedaci, P. Genevet, S. Barland, M. Giudici, J. Tredicce, G. Tissoni, and L. A. Lugiato, "Microresonator Defects as Sources of Drifting Cavity Solitons," Phys. Rev. Lett. **102**, 163901 (2009).
22. E. Caboche, S. Barland, M. Giudici, J. Tredicce, G. Tissoni, and L. A. Lugiato, "Cavity-soliton motion in the presence of device defects," Phys. Rev. A **80**, 053814 (2009).
23. B. Schäpers, T. Ackemann, and W. Lange, "Properties of feedback solitons in a single-mirror experiment," IEEE J. Quantum Electron. **39**, 227–237 (2003).
24. I. Babushkin, M. Schulz-Ruhtenberg, N. A. Loiko, K. F. Huang, and T. Ackemann, "Coupling of polarization and spatial degrees of freedom of highly divergent emission in broad-area square vertical-cavity surface-emitting lasers," Phys. Rev. Lett. **100**, 213901 (2008).
25. M. Schulz-Ruhtenberg, Y. Tanguy, R. Jäger, and T. Ackemann, "Length scales and polarization properties of annular standing waves in circular broad-area vertical-cavity surface-emitting lasers," Appl. Phys. B **97**, 397–403 (2009).
26. H. Pier and E. Kapon, "Photon localization in lattices of coupled vertical-cavity surface-emitting lasers with dimensionalities between one and two," Opt. Lett. **22**, 546–548 (1997).
27. S. Hoogland, J. J. Baumberg, S. Coyle, J. Baggett, M. J. Coles, and H. J. Coles, "Self-organized patterns and spatial solitons in liquid-crystal microcavities," Phys. Rev. A **66**, 055801 (2002).
28. C. Denz, S. J. Jensen, M. Schwab, and T. Tschudi, "Stabilization, manipulation and control of transverse optical patterns in a photorefractive feedback system," J. Opt. B: Quantum Semiclass. Opt. **1**, 114–120 (1999).
29. B. Gütlich, H. Zimmermann, C. Denz, R. Neubecker, M. Kreuzer, and T. Tschudi, "Forcing and control of localized states in optical single feedback systems," Appl. Phys. B **81**, 927–936 (2005).
30. U. Bortolozzo and S. Residori, "Storage of localized structure matrices in nematic liquid crystals," Phys. Rev. Lett. **96**, 037801 (2006).
31. B. Gütlich, H. Zimmermann, C. Cleff, and C. Denz, "Dynamic and static position control of optical feedback solitons," Chaos **17**, 037113 (2007).
32. F. Pedaci, P. Genevet, S. Barland, M. Giudici, and J. R. Tredicce, "Positioning cavity solitons with a phase mask," Appl. Phys. Lett. **89**, 221111 (2006).
33. M. Grabherr, M. Miller, R. Jäger, R. Michalzik, U. Martin, H. J. Unold, and K. J. Ebeling, "High-Power VCSEL's: Single Devices and Densely Packed 2-D-Arrays," IEEE J. Sel. Top. Quantum Electron. **5**, 495–502 (1999).
34. M. Schulz-Ruhtenberg, I. Babushkin, N. A. Loiko, T. Ackemann, and K. F. Huang, "Transverse patterns and length-scale selection in vertical-cavity surface-emitting lasers with a large square aperture," Appl. Phys. B **81**, 945–953 (2005).
35. M. Schulz-Ruhtenberg, Y. Tanguy, K. F. Huang, R. Jäger, and T. Ackemann, "Control of the spatial emission structure of broad-area vertical-cavity surface emitting lasers by feedback," J. Phys. D: Appl. Phys. **42**, 055101 (2009).
36. P. V. Paulau, D. Gomila, T. Ackemann, N. A. Loiko, and W. J. Firth, "Self-localized structures in vertical-cavity surface-emitting lasers with external feedback," Phys. Rev. E **78**, 016212 (2008).
37. N. Radwell, C. McIntyre, A. Sroggie, G.-L. Oppo, W. Firth, and T. Ackemann, "Switching spatial dissipative solitons in a VCSEL with frequency selective feedback," Eur. Phys. J. D **59**, 121–131 (2010).
38. C. H. Henry, "Theory of the linewidth of semiconductor lasers," IEEE J. Quantum Electron. **18**, 259–264 (1982).

#129452 - $15.00 USD Received 4 Jun 2010; revised 11 Aug 2010; accepted 11 Aug 2010; published 19 Oct 2010

39. A. J. Scroggie, W. J. Firth, and G.-L. Oppo, "Cavity-soliton laser with frequency-selective feedback," Phys. Rev. A **80**, 013829 (2009).
40. F. Pedaci, G. Tissoni, S. Barland, M. Giudici, and J. R. Tredicce, "Mapping local defects of extended media using localized structures," Appl. Phys. Lett. **93**, 111104 (2008).

1. Introduction

Soliton-like wave packets of light are intensively investigated for fundamental interest in self-localization and due to possible applications in all-optical processing [1–6]. Among these, spatial dissipative solitons in broad-area semiconductor microcavities (cavity solitons or CS) received considerable interest [3–5] because semiconductor devices seem to be particulary suited for all-optical processing due to their high nonlinearity, established, compact technology and relatively fast fundamental timescales. Further recent progress lead to the realization of CS in self-sustained semiconductor lasers without the need for an optical input of high temporal and spatial coherence [7–12]. In such a system the CS act as small coherent lasing islands – micro-lasers –, each of which is bistable between on and off states, and may be switched on and off independently by an external optical control beam [7, 8, 10].

As a self-localized state, a CS can exist anywhere in a translationally invariant system but couples on the other hand easily to any perturbation of the translational symmetry leading to a drift motion which only stops at a local extremum of the perturbation where the coupling of the odd translational mode of the CS to the (locally) even perturbation vanishes [5, 13–16]. Hence, it is probably not surprising that in all experimental realizations of CS in semiconductor microcavities, the CS always appear in the same position and while small displacements from this initial position are possible by applying additional perturbations, the shift range is usually limited [3, 8–11, 17]. It is also commonly observed experimentally that the CS appear spontaneously if a stress parameter is varied and that each CS has a different threshold [11, 18, 19]. In contrast, from the theory it is expected that no CS appears spontaneously on the background state during a parameter sweep through the bistable region because the excitation of a CS needs a hard perturbation [5]. At the edge of the stable range of the background state the system should move then into an another homogeneous state or an extended pattern (in case of a modulational instability; see [5] for a review).

Previous work performed in semiconductor micro-cavities reported micron-scale cavity parameter variations (defects) which were shown to play a role in pattern selection in semiconductor micro-cavities [20]. References [21, 22], in line with earlier investigations in sodium vapor [23], indicate that at least some kind of 'defects' also have an influence on threshold characteristics of solitons, i.e. solitons nucleate in the defects and are then carried away along phase gradients in the holding beam. Investigations into broad-area VCSELs also indicated that the spatial coherence of on-axis emission is limited by an uncontrolled spatial variation of cavity parameters [24, 25]. Disorder limits also the coherence of VCSEL arrays [26].

The future applications of these systems rely on the ability to accurately control the CS, in both position and threshold. Thus the presence of spatial defects is a limiting factor for potential applications and it is therefore crucial to achieve an understanding of the defects as well as to attempt to compensate for them, thereby returning to a more ideal and homogeneous laser system.

Spatial disorder is of course present to some degree in all spatially extended nonlinear systems and its effects have been seen previously, e.g., in liquid crystals [27] and photorefractive crystals [28]. Its effect on self-organization is probably best investigated in so-called liquid crystal light valves (LCLV) [16, 29–31]. Large-scale inhomogeneities in the sensitivity of the device can lead to solitons only existing in small areas of the whole aperture. It was shown that the phase shift induced by a suitably shaped spatial modulation of an external control beam can be

#129452 - $15.00 USD Received 4 Jun 2010; revised 11 Aug 2010; accepted 11 Aug 2010; published 19 Oct 2010

used to compensate that inhomogeneity to a large extent leading to the formation of CS essentially everywhere in the transverse aperture [29]. Positioning of the solitons can be controlled by imprinting a spatial modulation stronger than the pinning defects leading to rather regular arrays of solitons in atomic vapor cells, LCLVs and semiconductor microcavities [15, 30–32]. It turns out, however, that it is still a challenge to ensure that all the solitons in these induced arrays are simultaneously bistable [15, 31, 32].

In this paper we concentrate on the effect of spatial disorder on broad-area VCSELs. The VCSEL is coupled to a volume Bragg grating (VBG) which provides frequency-selective feedback to support bistability necessary for a cavity soliton laser. We will demonstrate the first disorder compensation in a cavity soliton laser by using a spatial light modulator to influence locally the cavity resonance of the VCSEL. As a result CS which were not simultaneously bistable without control will have overlapping hysteresis loops with control.

2. Experimental setup

Figure 1 shows the experimental setup, which has three main components: a cavity soliton laser, a compensation beam and a detection arm. The cavity soliton laser is composed of a broad-area VCSEL with frequency-selective feedback from a VBG. The VCSEL has a 200 μm diameter circular aperture. It is temperature tuned to have a cavity resonance at around 978 nm in order to approach the reflection peak of the VBG which is centered on 978.2 nm and 0.11 nm wide.

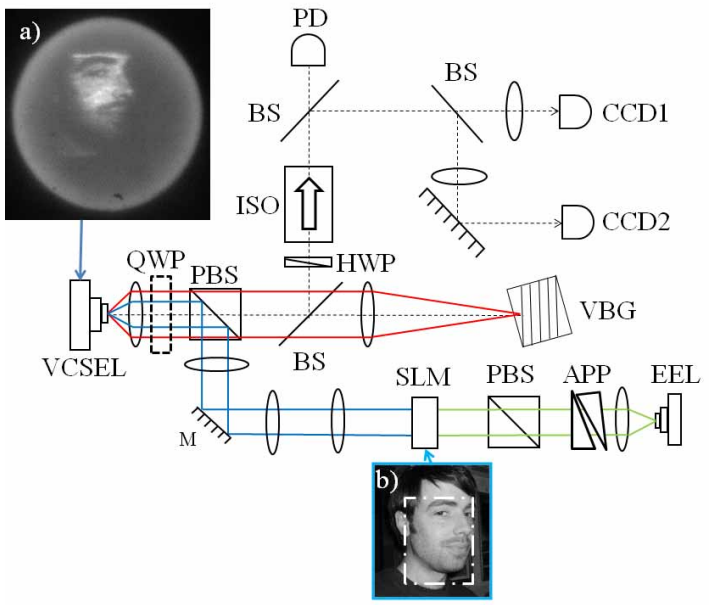

Fig. 1. Experimental Setup. APP: Anamorphic prism pair, BS: Beam splitter, CCD1(2): Charge coupled device camera imaging a near (far) field plane of the VCSEL gain region, EEL: Edge emitting laser, HWP: Half wave plate, ISO: Optical isolator, PBS: Polarizing beam splitter, PD: Photodiode, QWP: Quarter wave plate, SLM: Spatial light modulator, VBG: Volume Bragg grating, VCSEL: Vertical-cavity surface-emitting laser. a) Near field image of the VCSEL showing the aperture of the VCSEL being illuminated by the spatially modulated laser beam from the SLM with input b), the modulation image displayed on the SLM. The white outline in b) indicates the region which is illuminated by the expanded EEL beam.

#129452 - $15.00 USD Received 4 Jun 2010; revised 11 Aug 2010; accepted 11 Aug 2010; published 19 Oct 2010

The VCSEL and VBG are coupled via an external self-imaging cavity with length 61.6 cm [11].

The compensation beam is derived from a spatially modulated edge-emitting laser (EEL) diode. The diode emits at wavelengths around 978 nm and its wavelength is tunable via temperature. The beam from the diode is collected by a collimating lens and then reshaped by an anamorphic prism pair. The beam is then expanded to a size of approximately 10 mm $\times$ 10 mm, which is insufficient to fill the entire aperture of the used spatial light modulator (SLM) but is kept small to attempt to keep the intensity of the beam high. The beam is then horizontally polarized by a polarizing beamsplitter cube. Afterwards it is spatially modulated by the Holoeye LC 2002 transmissive SLM. The SLM has a design wavelength of 532 nm, however some modulation is still present at 980 nm though it is smaller than 15%. This lack of modulation will turn out to be a significant restriction on the performance of the system. The total optical power which reaches the VCSEL front mirror is $<$1 mW when the whole SLM is set to transmit. The transmission aperture is 25.6 mm $\times$ 19.2 mm and contains 800 $\times$ 600 pixels.

The SLM induces a spatially modulated polarisation rotation upon the incident beam and when placed between crossed polarizers, the rotation is converted to an intensity modulation. After the beam passes through the SLM, it is demagnified to match the size of the VCSEL aperture and coupled into the cavity soliton laser (CSL) cavity via a polarizing beam splitter. A consequence of the polarization sensitive injection is that the compensation beam does not propagate in the external cavity. This however also means that the compensation beam is not visible in the detection arm. To align the compensation beam we therefore have to place a quarter-wave plate before the VCSEL in order to see the alignment of the compensation beam in relation to the VCSEL aperture. The quarter-wave plate is removed when the experiment commences. Note that there is no coherent interaction between the beam propagating in the external cavity and the compensation beam even if they are close in frequency because they are orthogonally polarized.

An example of the effect and resolution of the compensation beam is shown in Fig. 1a and Fig. 1b. If we apply the image shown in Fig. 1b then the modulation shown in Fig. 1a is achieved at the VCSEL surface. The circular disk seen in Fig. 1a is the 200 μm diameter aperture of the VCSEL showing spontaneous emission below threshold. The entire aperture is not illuminated by the EEL beam in order to achieve a reasonable compromise between intensity and spatial range covered. The enhancement of brightness around the perimeter of the laser is due to current crowding at the oxide aperture [33].

The detection system is isolated from the laser cavity by an optical isolator. A photodiode records time-averaged intensity and two charge-couple device (CCD) cameras monitor the reimaged near and far field planes of the VCSEL cavity.

3. Spatial inhomogeneities and threshold conditions

The ideal cavity in a VCSEL is transversely homogeneous. In reality though there is a spatial variation of parameters which breaks the translational symmetry. This spatial variation of parameters will be referred to as spatial disorder or defects.

The disorder is not visible in the spontaneous emission, in large aperture devices the spontaneous emission is essentially homogeneous across the aperture (see also Fig. 1a). There is some minor manifestation of disorder in the distribution of off-axis lasing in the free running laser case (on-axis emission is not obtained in these broad-area lasers) however the disorder only really becomes apparent when frequency selective-feedback is introduced. In this case CS are formed and each has a different frequency, this supports that the defects we are mainly concerned with are not dark line or other gain defects which cause individual or several VCSEL units to be useless, but disorder in the cavity resonance affecting the phase, as we will argue in detail below.

#129452 - $15.00 USD Received 4 Jun 2010; revised 11 Aug 2010; accepted 11 Aug 2010; published 19 Oct 2010

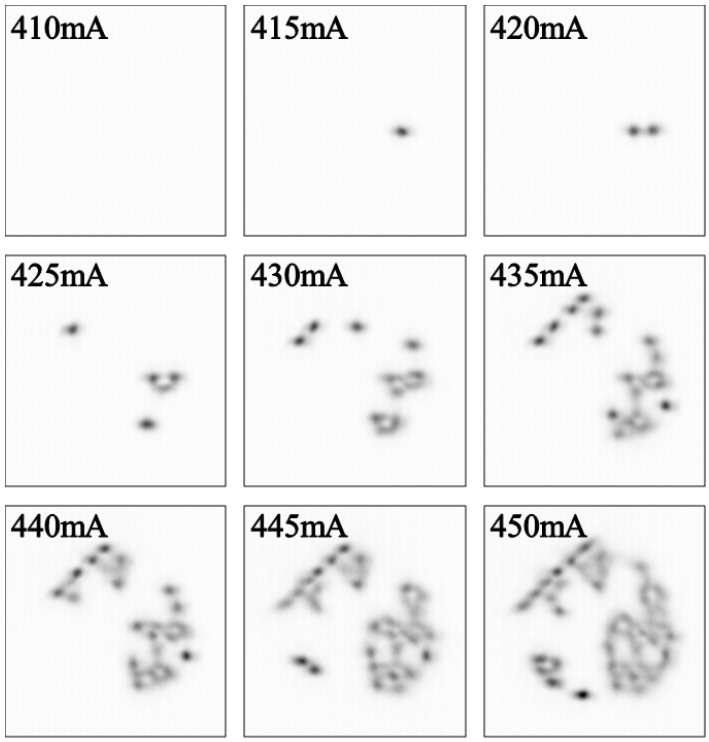

Fig. 2. Negative intensity (black corresponds to high intensity) near field images of the VCSEL gain region. Pictures taken at the inset currents. Pictures taken from the CSL system in [11].

Initially, the cavity resonance frequency of the VCSEL is higher than the reflection peak of the VBG. If the current into the VCSEL is increased, not only the gain properties change but the resonance shifts to lower frequencies with a rate of 0.0035 nm/mA due to Ohmic heating. Figure 2 illustrates this change of detuning of the frequency-selective feedback (see also [11]). For low currents (410 mA) there is no lasing, and only spontaneous emission. Increasing the current (415 mA) causes a lasing spot to appear, which is a CS. Increasing the current further CS switch on at different locations (425 mA and 430 mA) until at some higher current values the initial spots convert to extended lasing states (‘patterns’, 435 mA). These are also distinguished from the CS by the fact that they are emitting off-axis and at higher frequency. At still higher currents, patterns extend over large parts of the VCSEL. (Another way to visualize the different thresholds for separate CS is given in Fig. 6 (solid line).)

The spatial distribution and relative threshold of each lasing island remains constant for repeated current ramps and is interpreted to be the manifestation of a spatially varying cavity resonance across the aperture of the VCSEL. The parts of the cavity which are detuned closest to the feedback frequency begin to lase first, and thus provide insight into the distribution of defects. Details are under investigation but we propose that the shape which these patterns adopt provides a mapping of the cavity resonance conditions.

The interpretation of the mechanism which dictates the threshold of the CS is schematically outlined in more detail in Fig. 3. In the sketch the grating wavelength λ_g is fixed. The so-called ’cold-cavity‘ VCSEL resonance is initially situated at the leftmost solid curve. The square-root shaped curve emerging towards the left (lower wavelengths, higher frequencies) indicates the

#129452 - $15.00 USD Received 4 Jun 2010; revised 11 Aug 2010; accepted 11 Aug 2010; published 19 Oct 2010

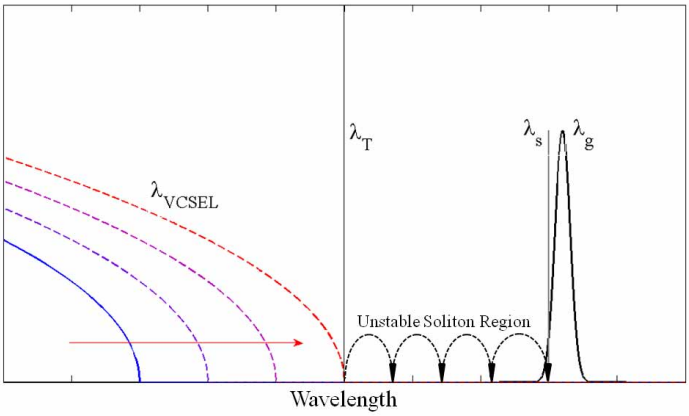

Fig. 3. Schematic diagram of the proposed CS switching mechanism. λ_g is the central reflection wavelength of the VBG with the curve denoting the reflection band. λ_s is the final wavelength of the stable CS, λ_T is the threshold wavelength and λ_{VCSEL} are the cavity modes of the VCSEL. The arrow corresponds to the wavelength shift induced by increasing VCSEL pump current. Wavelengths are only included for rough visualization and are not accurate. The curves on the left are the cavity modes of the VCSEL, with the lines denoting the dispersion relation of threshold wavenumber vs. λ for a plano-planar cavity.

wavenumber of the high-order VCSEL modes [34, 35].

Applying current to the VCSEL heats the cavity via Ohmic heating. This results in the cavity resonance wavelength red shifting along the straight arrow in Fig. 3. The red shift brings the VCSEL modes closer to the grating wavelength, hence increasing feedback, lowering the losses. When the resonance reaches a critical point, marked λ_T on Fig. 3, the VCSEL attempts to begin lasing. Lasing across the whole aperture is not stable in this regime however, and filaments are formed which self-localize via nonlinearities to a CS. The blue most wavelengths are not stable solitons either however, and in this region (marked 'unstable soliton region' on Fig. 3) the wavelength cascades through multiple unstable modes until the CS finally reaches a stable mode which is slightly blue detuned to the grating wavelength [36, 37].

Following the argument of Fig. 3 in which there is a threshold current at which the onset of the frequency cascade occurs, one would expect that for an ideal plano-planar VCSEL cavity all CS have the same threshold (dashed line in Fig. 4a), since all CS would have the same frequency and would tune with current at the same rate. However in real systems, such as that in Fig. 2, the CS do not have the same threshold. The interpretation is that there is a spatial distribution of cavity resonance (dotted curves in Fig. 3 and solid line in Fig. 4a), leading to the most reddish parts of the cavity reaching threshold first and producing a distribution of CS threshold frequencies. This disorder also has a pinning effect on the CS (grey spots shown in Fig. 4a) since the CS are essentially trapped by the cavity resonance gradients which surround the trap. The traps not only dictate where the CS appear at switch-on but limit the spatial range of their existence.

The net effect of spatial disorder on CS is therefore separation of thresholds, limiting the number of simultaneously bistable CS, and pinning to specific locations, all of which severely limit potential applications. Hence we will try to compensate for this disorder.

#129452 - $15.00 USD Received 4 Jun 2010; revised 11 Aug 2010; accepted 11 Aug 2010; published 19 Oct 2010

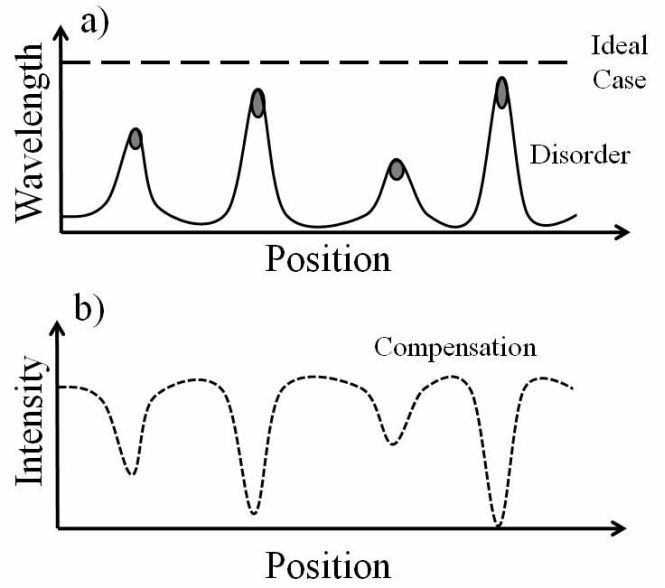

Fig. 4. a) Sketch of the spatial variation of cavity resonance in a VCSEL. The dashed line represents the situation for an ideal plano-planar cavity. The lower solid line indicates how the resonance might vary in a real laser. Grey dots indicate CS pinning regions (traps). b) Externally injected laser beam intensity modulation required to compensate for the cavity resonance variation shown in a).

4. Concept of disorder compensation by induced refractive index changes

The spatial disorder may be compensated for by spatially modulating the effective (i.e. averaged over the longitudinal structure) refractive index $n(x,y)$ of the VCSEL cavity to compensate for the spatial disorder in cavity length $L(x,y)$ (in reality, the VCSEL will have spatial disorder in refractive index and layers thicknesses but it is sufficient for our purposes to speak of an effective cavity length $L(x,y)$ alone):

$$n(x,y) = \frac{m\lambda_0}{2L(x,y)}\,, \tag{1}$$

where m is the mode order and λ_0 the design vacuum wavelength. This compensation can be achieved by injection of an external laser beam. This beam would alter the number of carriers, altering the refractive index via phase-amplitude coupling as described phenomenologically by Henry's α-factor [38]. In quantum well materials, decreasing the carrier density results in an increase in refractive index. This refractive index change alters locally the optical path length, resulting in a cavity resonance shift as desired by Eq. (1). Since semiconductors are a saturable and nonlocal medium the connection between input intensity and the resulting phase shift is not straightforward but quantitative calculations can be based on suitable rate equations, e.g. [39]. Alternatively, one can calibrate the effect experimentally which is the approach we choose for this first demonstration.

Two choices for external laser wavelength are apparent. The first choice would be to use a beam with a frequency outside the stop-band of the Bragg mirrors of the VCSEL in order to have high efficiency without the sensitivity of resonance effects. The beam should be absorbed in the active area and not in the Bragg mirrors. Hence, a wavelength in the 900–920 nm region is a good choice. Absorption of photons at this wavelength results in the creation of additional

#129452 - $15.00 USD Received 4 Jun 2010; revised 11 Aug 2010; accepted 11 Aug 2010; published 19 Oct 2010

carriers to the VCSEL. This results in a decrease of refractive index, a blue detuning of the cavity resonance, and thus increases the threshold of a CS. Hence, by aiming more power on the most reddish CS with the lowest thresholds, the thresholds should be equalized at a higher current (note that this is opposite to the situation depicted in Fig. 4). However, experimental investigations with a 905 nm control beam showed that the thresholds of the CS were actually reduced indicating that the cavity resonances were actually tuning towards the red. This can be understood by the fact that in practice there is also a thermal component to the refractive index change due to the dissipation of the excess energy of the 905 nm photon compared to the 980 nm band edge leading to heating. The experiments indicate that the thermal red-shift dominates over the carrier-induced blue-shift. This interpretation was reinforced when the locality of a 905 nm beam was tested, as the effect of a local control beam was found to have long-range influence over the entire VCSEL aperture. There was also a delay of some 25 ms between the application of the 905 nm beam and the response of the CS. Both of these phenomena are compatible with a thermal dissipation mechanism which make a 905 nm control beam unsuitable for spatial compensation applications.

A 978 nm EEL was then used for the compensation beam. It needs to be injected within the resonance width of the VCSEL cavity because it is rejected by the high-reflectivity Bragg output coupler otherwise. In that wavelength range the VCSEL is inverted, hence injection actually reduces the carrier density, increases the refractive index, red-shifts the carrier resonance and hence lowers the thresholds. This situation is indicated in Fig. 4. There is no injection at the position of the CS with the lowest threshold (the most reddish CS) and the injection intensity is increased for the other CS in dependence on threshold such that the cavity resonance is equalized at the level of the first CS (lowest threshold situation).

5. Results: Local threshold control

Indeed, a 978 nm beam was found to be capable of lowering the threshold of a CS and the effect was found to be also local, as can be seen in Fig. 5. Figure 5 is produced by using the SLM to filter out a small circular beam, of similar size to a CS, and directing it close to the

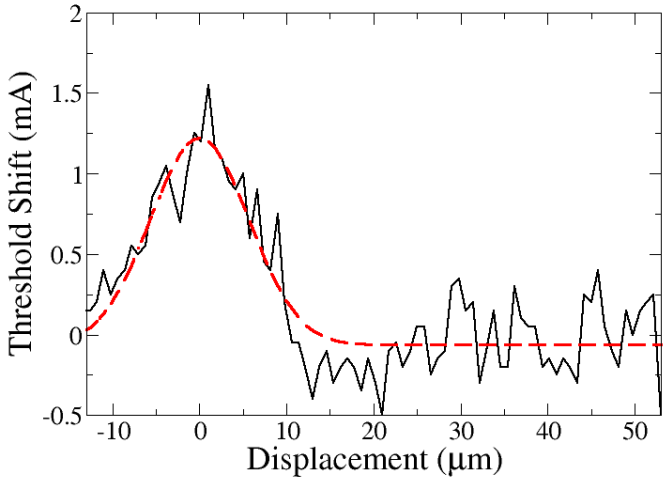

Fig. 5. Reduction in threshold current of a CS induced by the application of a local 980 nm SLM beam for varying distance to the CS peak. Line is experimental data, dashed red curve is a Gaussian fit to the data.

#129452 - $15.00 USD Received 4 Jun 2010; revised 11 Aug 2010; accepted 11 Aug 2010; published 19 Oct 2010

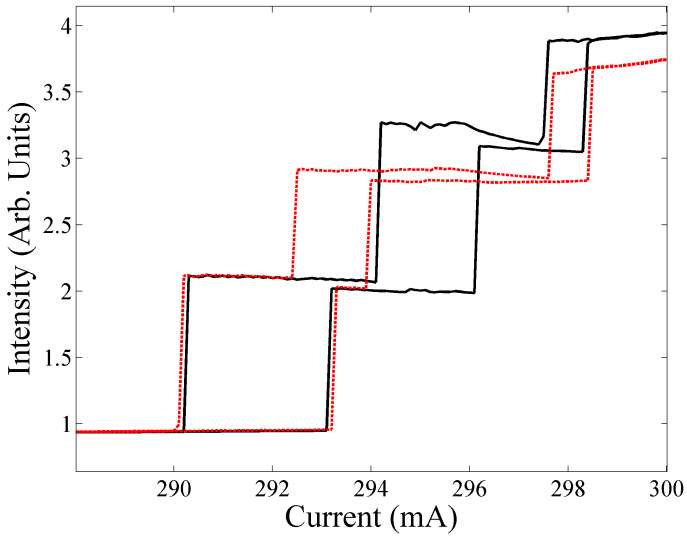

Fig. 6. Light-Current (LI) characteristics for the system before (solid line) and after (dotted line) the application of the SLM beam.

location of a known CS. The light-current characteristic (LI-curve, see, e.g., the solid line in Fig. 6) for this CS is recorded with the compensation beam switched off, and the 'natural' threshold current is noted. The LI-curve is then repeated with the compensation beam switched on and the new threshold is noted. The LI-curve is then recorded a third time with the compensation beam off again. This is to compensate for any drift of the threshold which occurs due to macroscopic thermal fluctuations. These three LI-curves are compared to obtain the threshold reduction induced by the compensation beam for a particular position of the beam. The beam is then scanned spatially across the CS and the threshold reduction is noted at each point.

Figure 5 shows that the threshold reduction is largest when the beam is applied directly on top of the CS, as expected. The threshold reduction reduces rapidly as the beam is moved away from the center of the CS ($1/e^2$ radius 5 μm) which indicates that the threshold reduction effect with a 980 nm compensation beam is indeed local.

Since the thresholds of the CS are governed by the local cavity resonance it is possible to assess the viability of any compensation scheme by monitoring the relative thresholds of several CS. It should be shown that any compensation scheme is capable of locally adjusting thresholds such that a number of CS which have differing thresholds and bistable regions, have their thresholds shifted such that they share a common region of bistability.

To this end the system is set up such that it produces three CS with similar thresholds. An LI-curve for these CS is measured, and can be seen as the solid curve in Fig. 6. It shows that the first CS has a threshold around 293 mA, the second around 296 mA and a third around 298 mA. Figure 7a shows the position of the CS when the system is biased in the region where the two CS with lowest threshold are present. A compensation beam is then placed on top of the CS with the second lowest threshold (arrow in Fig. 7b) and the LI-curve is measured again. The near-field intensity distribution with the compensation beam on is shown in Fig. 7b. The dotted curve in Fig. 6 shows the LI-curve which is observed when the compensation beam is applied. There is a clear reduction in threshold current for the second CS, while the first and third remain unchanged. The shift of threshold of the middle CS shows that the system is capable of altering the cavity resonance of the VCSEL, and the lack of shift for the other two CS shows that the

#129452 - $15.00 USD Received 4 Jun 2010; revised 11 Aug 2010; accepted 11 Aug 2010; published 19 Oct 2010

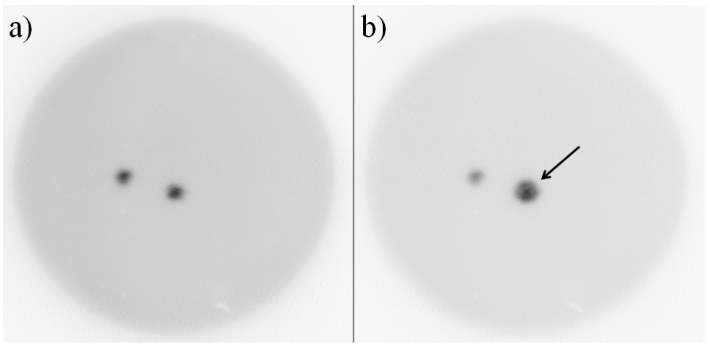

Fig. 7. Negative intensity (black corresponds to high intensity) near field images of the VCSEL gain region. a) Two CS shown inside the circular VCSEL aperture. b) Application of the SLM beam on top of the right CS. The arrow shows the location of the SLM beam. $I = 297$ mA.

system is only shifting cavity parameters locally, which are the two ingredients for a successful compensation scheme. The first and second CS are now simultaneously bistable in a robust current range which they were not before. The observed threshold change of about 2 mA can be related to a frequency change using the rate of 1.1 GHz/mA by which cavity resonances shift with current for the free-running laser. The result is a shift of about 2.2 GHz, which seems to be a in reasonable agreement with findings on the size of inhomogeneities in [40].

The reported measurements confirm the feasibility of a local threshold correction of semiconductor CS but the system has two main limitations in its current implementation. The first problem is that as the threshold of a CS is reduced by the application of the SLM beam, the bistable range also reduces. This can be seen in Fig. 6 as the difference in bistable widths between the solid line and the dotted line. The width reduces in proportion to the reduction in threshold which places a restriction on how far the threshold may be reduced before bistability is lost.

The second issue with the current realisation is that the power level available for control is rather low due to the low modulation efficiency of the SLM used. To achieve a sizable threshold reduction with these low powers, the SLM beam must be tuned in frequency to be resonant with the VCSEL cavity. Since the resonance condition differs between the locations of different CS, it is impossible to have good injection efficiency for more than one CS at a time, making threshold reduction of multiple CS difficult at these power levels. However, a more intense SLM beam would be able to affect CS threshold further off-resonance. This is supported by observations of switch-on thresholds of CS with an external, pulsed laser beam which demonstrate that one can trade detuning versus power [7].

6. Conclusion

In conclusion, we have outlined the constraints which spatial disorder imposes upon CS, limiting the freedom of location, spreading their thresholds, and thus causing problems for potential applications. The major origin of spatial disorder was inferred to be a spatial variation of cavity resonance. Therefore a scheme in which the cavity resonance is shifted locally via a carrier-induced refractive index change such that the thresholds of different CS may be aligned was realized. The effectiveness of the current realization is limited by the power available and the resulting reliance on the individual VCSEL resonance conditions. However, an increase in power should allow the scheme to achieve spatial disorder compensation over the full aperture. We expect that a compensation of the threshold conditions leads also to reduction of the spatial pin-

#129452 - $15.00 USD Received 4 Jun 2010; revised 11 Aug 2010; accepted 11 Aug 2010; published 19 Oct 2010

ning effects. The ultimate goal would be to produce a spatially smoothly varying control beam to counteract the inhomogeneities at any location. This would allow further, more focussed investigations into specific applications. After compensation is reached, additional modulations like in [30–32] might be superimposed on top of the compensating beam to control the locations and/or thresholds of CS at will in order to achieve a desired pattern or effect. If the superimposed modulations are random, one might investigate the effects of different strengths of disorder in a controlled way.

In addition, the shape of the necessary modulation for compensation will provide a 'map' of the spatial disorder of the VCSEL resonance and might be a useful diagnostic tool to characterize and understand growth defects in VCSELs. There is a close connection to other approaches to use the sensitivity of solitons to disorder in a kind of 'soliton force microscope' to learn about the parameters of photonic microcavities [5, 40].

Acknowledgement

We are grateful for useful discussions with W. J. Firth and G.-L. Oppo, to R. Jäger (Ulm Photonics) for supplying the devices and to the Deutscher Akademischer Austausch Dienst, the British Council, and the Royal Society (London) for financial support. Initial work was supported also by the EU FP6 STREP FunFACS. NR is supported by an EPSRC doctoral training account.

#129452 - $15.00 USD Received 4 Jun 2010; revised 11 Aug 2010; accepted 11 Aug 2010; published 19 Oct 2010